Engineering Fracture Mechanics 78 (2011) 1277–1288

Contents lists available at ScienceDirect

Engineering Fracture Mechanics

journal homepage: www.elsevier.com/locate/engfracmech

Fracture toughness of foams with tetrakaidecahedral unit cells using finite element based micromechanics

Prasanna Thiyagasundaram [1], Junqiang Wang [2], Bhavani V. Sankar *, Nagaraj K. Arakere

Department of Mechanical and Aerospace Engineering, PO Box 116250, University of Florida, Gainesville, FL 32611-6250, USA

ARTICLE INFO

Article history:
Received 27 July 2010
Received in revised form 11 December 2010
Accepted 4 January 2011
Available online 15 January 2011

Keywords:
Cellular materials
Foams
Fracture toughness
Micromechanics
Tetrakaidecahedral unit cell

ABSTRACT

Fracture toughness of open-cell foams consisting of tetrakaidecahedral unit cells is predicted by simulating crack propagation using a finite element (FE) based micromechanical model. The inputs to the model are the geometric parameters required to model the repeating unit cell and tensile strength of the foam ligament or strut. Cracks are created by removing certain number of cells pertaining to a crack length. The FE model consists of a local micro-scale region surrounding the crack tip. For an assumed stress intensity factor, the displacements along the boundary of the local model are calculated based on linear elastic fracture mechanics for orthotropic materials. The stresses in the ligaments ahead of the crack tip calculated from this micro-model in conjunction with the tensile strength of the strut material are used to predict fracture toughness. A parametric study with different micro-model sizes and different crack lengths is performed to check for convergence of predicted Mode-I, Mode-II and mixed mode fracture toughness values. The effect of applying rotations as additional boundary conditions along with translational displacement boundary conditions on the predicted fracture toughness values is also studied.

1. Introduction

Cellular materials are made up of a network of beam or plate-like structures. There are a number of cellular materials that occur in nature, such as honeycombs, wood, bone, and cork. Cellular materials can offer high thermal resistance, low density, and high energy-absorption. Foams are a class of cellular solids, generally made by dispersing gas into a liquid and then cooling it to solidify. Foams are categorized as open-cell and closed-cell foams. Depending on the solid materials made into foams, they are also categorized as polymeric, metallic, and ceramic foams, etc. Due to developments in material science and manufacturing techniques, advanced foams have great potential for use in automobile, aircraft, and space vehicle structures. A special example is the application in thermal protection system (TPS) of space vehicles. Most of the available literature focuses on thermo-elastic constants of foams, whereas fracture and failure have been paid very little attention. Thus there exists an urgent need for the study of crack propagation behavior and fracture toughness of foams. Since the representative volume element or unit cell of many types of foams such as the carbon foam.

Fig. 1 could be well approximated as a tetrakaidecahedron (Fig. 2), fracture toughness of tetrakaidecahedral foams will be studied in this paper.

* Corresponding author.
E-mail addresses: pthiyaga@ufl.edu (P. Thiyagasundaram), sankar@ufl.edu (B.V. Sankar), nagaraj@ufl.edu (N.K. Arakere).
[1] Present address: Intel Corporation, Portland, Oregon, United States.
[2] Present address: Belcan Engineering Group Inc., Cincinnati, Ohio, United States.

0013-7944/$ - see front matter © 2011 Elsevier Ltd. All rights reserved.
doi:10.1016/j.engfracmech.2011.01.003

Nomenclature

D	length of the side of equilateral triangle cross section of the strut
E_{001}, E_{010}, E_{100}	elastic moduli of the foam in the lattice vector directions
G_c	critical strain energy release rate
K_I	Mode I stress intensity factor
K_{Ic}	Mode-I fracture toughness
K_{II}	Mode II stress intensity factor
K_{IIc}	Mode-II fracture toughness
l	length of each strut in the tetrakaidecahedron unit cell
ω_{xy}	rotations in the XY plane (Fig. 3)
p, q, s	parameters dependent on the material constants of the foam
ψ	phase angle used as a measure of mode mixity
r	radial distance of points in the K-field boundary from the crack tip
S_{ij}	compliance matrix coefficients of the foam
ρ^*	density of the foam
ρ_s	density of the solid material
σ_{tip}	maximum principal stress in the strut in the vicinity of crack tip
σ_u	ultimate tensile strength of strut
θ	angle measured between the positive X-axis and line joining the crack tip to the points in the K-field boundary
u	displacement in the X-direction (Fig. 3)
,v	displacement in the Y-direction (Fig. 3)

It has been accepted for a long time that a tetrakaidecahedron, packed in a BCC structure, satisfies the minimum surface energy condition for mono-dispersed bubbles [1]. Only in 1994 a little better example with smaller surface energy was found [2]. The tetrakaidecahedral foams have held the interest of researchers for decades. Microcellular graphitic carbon foams were first developed at the US Air Force Research Laboratory in the 1990s [3]. The repeating unit cell of this foam can be approximated by a regular tetrakaidecahedron [4]. Micromechanical models have been used to predict mechanical properties such as Young's modulus, bulk modulus, yield surface, etc. Linear elastic behavior of low-density tetrakaidecahedral foams has been studied [5,6] and analytical model of elastic moduli has been developed [7]. Based on this analytical model, a fracture model for rigid polyurethane foam was derived analytically [8]. Nonlinear elastic response of the foams was studied under compressive loading and a failure surface was defined [9]. However, not much work has been done on predicting the fracture toughness of tetrakaidecahedral foams.

The most important parameter of cellular materials is the relative density $\bar{\rho} = \rho^*/\rho_s$, where ρ^* is the density of cellular medium and ρ_s the solid density, which is the density of the material that constitutes the struts or plates of the cell. The relative density is a measure of solidity, and most of the material properties depend on the relative density. Analytical methods for determining the mechanical and thermal properties of cellular solids are well documented. However, research on fracture

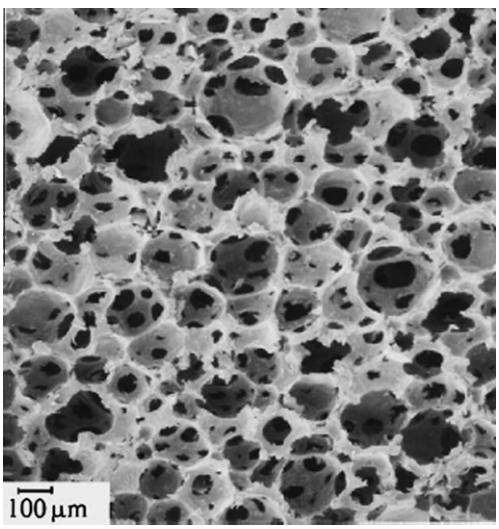

Fig. 1. Micrograph of an AFRL carbon foam [3].

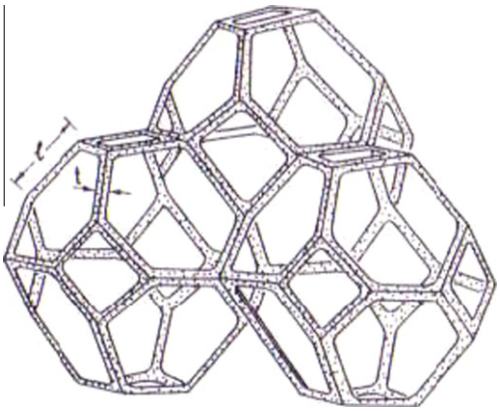

Fig. 2. Three tetrakaidecahedral cells with strut length l and thickness t in a BCC lattice [16].

behavior of foams is still at its infancy. A theoretical model [10] showed that the Mode-I fracture toughness of open-cell foams K_{Ic} was proportional to $(\rho^*/\rho_s)^3$ and Mode-II fracture toughness to $(\rho^*/\rho_s)^2$. This theoretical model was confirmed by studying several open-cell foams with short cracks [11,12]. Experiments were conducted to verify the theoretical model [13–15]. A comprehensive summary of mechanical properties of foams including fracture toughness could be found in Gibson and Ashby's book [16]. Recently, new results and models on fracture toughness of open-cell foams were presented [17–19].

FEM based micromechanics is one of the methods to investigate the fracture toughness of cellular materials. In this method displacement boundary conditions corresponding to a given stress intensity factor are calculated based on linear elastic fracture mechanics and applied to the micro-model. This approach was first used by Schmidt and Fleck [20] to study crack growth initiation and subsequent resistance to propagation in hexagonal honeycomb structures made from ductile cell walls. *K*-resistance curves were calculated under the assumption of small-scale yielding. Choi and Sankar [17,18] later used a similar approach for studying the fracture behavior of carbon foams. It has also been used to study the damage tolerance of elastic–brittle, 2-D isotropic lattices [21].

We use the same approach as Choi and Sankar [17,18] to determine the fracture toughness of tetrakaidecahedral foams. We directly apply displacements based on the *K*-field on the boundary of the micromechanical model. A commercial software – ABAQUS® – is used for FEM calculations and the input files of FEM are generated by MATLAB®. Furthermore, we investigate the effect of applying rotations as boundary conditions [21] in addition to prescribed translational displacement boundary conditions on the predicted fracture toughness.

2. Approach

Our approach is a global–local approach wherein the microstructure is modeled in detail near the crack tip (inner region), and boundary conditions are applied at far away points (outer region) according to continuum fracture mechanics (see

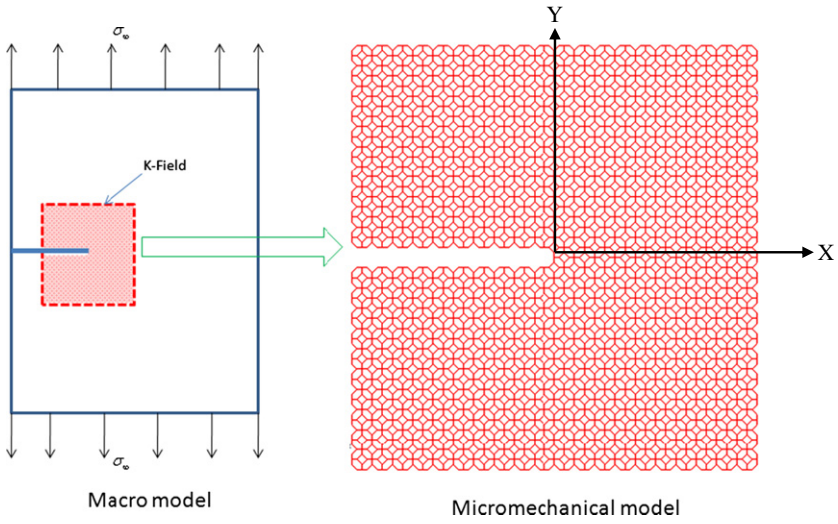

Fig. 3. Finite element micro-scale model of the cellular medium with a crack. The dimensions of the model depend on the number of unit cells used.

Fig. 3). The foam in the outer region is considered as a homogeneous orthotropic material. The microstructure of the inner region surrounding the crack tip is modeled in detail. The individual struts of the foam are modeled using finite elements. Consequently we assume that the displacement and stress fields in the outer region are well described by continuum fracture mechanics. Thus the displacements along the boundary of the inner and outer regions can be predicted by fracture mechanics equations for a given stress intensity factor. Obviously the inner region should be much larger than the strut dimensions. We verify this by performing a convergence study by varying the size of the inner region.

For foams made of brittle materials, once we know the stress intensity factor at macroscale and the corresponding maximum micro-scale tensile stresses in the struts ahead of the crack, we can calculate the fracture toughness of the foam by the following equation [17]:

$$\frac{K_I}{K_{Ic}} = \frac{\sigma_{tip}}{\sigma_u} \Rightarrow K_{Ic} = \frac{K_I}{\sigma_{tip}}\sigma_u \tag{1}$$

where K_I is the Mode I stress intensity factor, K_{Ic} is the Mode-I fracture toughness, σ_u is the tensile strength of struts or the foam ligaments, and σ_{tip} is the maximum tensile stress in the first unbroken strut ahead of the crack tip.

Sih and Liebowitz [22] determined the K-field in the vicinity of a crack tip in homogeneous orthotropic materials. We can directly apply displacements based on the K-field on the boundary of the microstructure. The displacement field near the crack tip for Mode I:

$$u(r,\theta) = K_I\sqrt{\frac{2r}{\pi}}\mathrm{Re}\left\{\frac{1}{s_1 - s_2}\left[s_1 p_2(\cos\theta + s_2\sin\theta)^{1/2} - s_2 p_1(\cos\theta + s_1\sin\theta)^{1/2}\right]\right\}$$
$$v(r,\theta) = K_I\sqrt{\frac{2r}{\pi}}\mathrm{Re}\left\{\frac{1}{s_1 - s_2}\left[s_1 q_2(\cos\theta + s_2\sin\theta)^{1/2} - s_2 q_1(\cos\theta + s_1\sin\theta)^{1/2}\right]\right\} \tag{2}$$

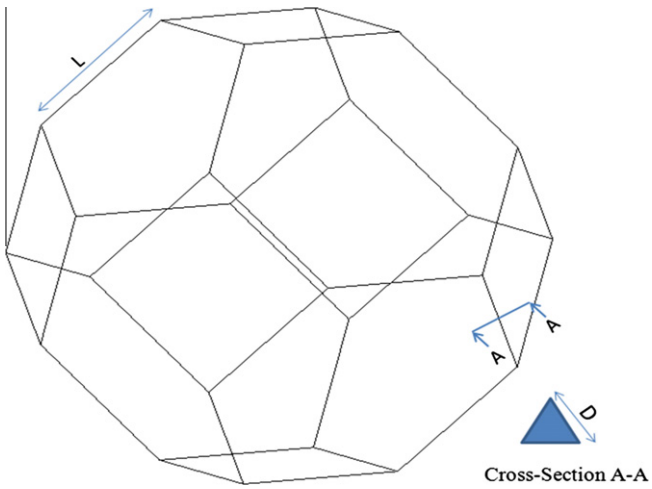

Fig. 4. A tetrakaidecahedral unit cell and the cross section of a strut.

Table 1
Properties of the strut chosen for Fracture toughness calculation.

	Property	Value
Material properties of the strut	Density, ρ_s (kg/m^3)	1650
	Elastic modulus, E_s (GPa)	23.42
	Poisson ratio, ν_s	0.33
	Tensile strength σ_u (MPa)	689.5
Geometry (Fig. 4–1)	L (mm)	1
	D (mm)	0.06
	Relative density	0.001653
Cross-section properties (equilateral triangle)	Cross sectional area, A (m^2)	1.5588×10^{-9}
	Moment of Inertia, I_x, I_y (m^4)	2.3382×10^{-19}
	Polar moment of Inertia, J (m^4)	4.6765×10^{-19}

The displacement field near the crack tip for Mode II:

$$u(r,\theta) = K_{II}\sqrt{\frac{2r}{\pi}}\mathrm{Re}\left\{\frac{1}{s_1 - s_2}\left[p_2(\cos\theta + s_2\sin\theta)^{1/2} - p_1(\cos\theta + s_1\sin\theta)^{1/2}\right]\right\}$$
$$v(r,\theta) = K_{II}\sqrt{\frac{2r}{\pi}}\mathrm{Re}\left\{\frac{1}{s_1 - s_2}\left[q_2(\cos\theta + s_2\sin\theta)^{1/2} - q_1(\cos\theta + s_1\sin\theta)^{1/2}\right]\right\} \quad (3)$$

Table 2
Elastic properties of the foam used in the current study.

	Property	Value
Elastic moduli	$E_x = E_x = E_z$ (Pa)	46.7×10^3
Poisson ratios	$v_{xy} = v_{yz} = v_{xz}$	0.498
Shear moduli	$G_{xy} = G_{yz} = G_{xz}$ (Pa)	14.9×10^3

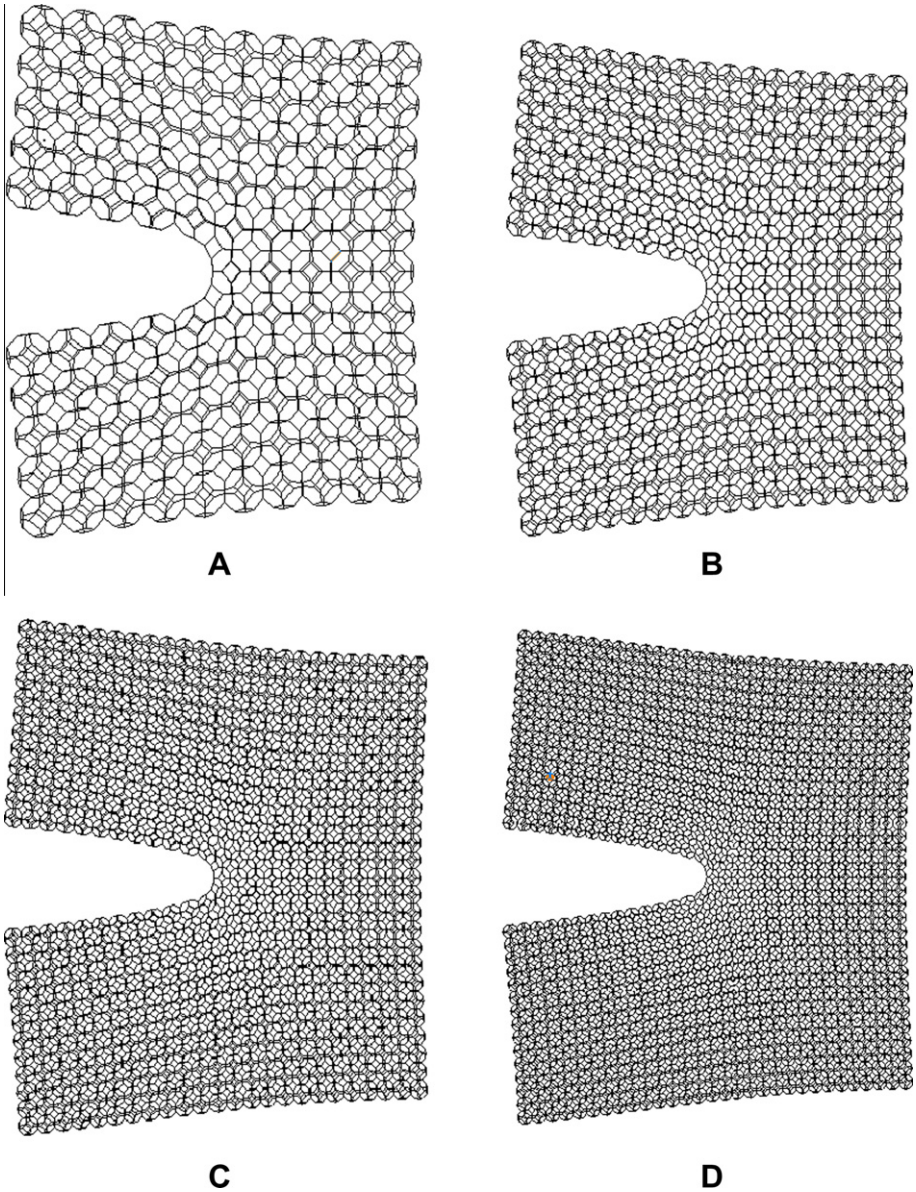

Fig. 5. Mode-I fracture toughness (deformed configurations). (A) 10(w) × 11(h), (B) 16(w) × 15(h), (C) 24(w) × 25(h), and (D) 30(w) × 31(h).

In the above relations the displacements are given as a function of polar coordinates r and θ instead of usual x and y for convenience. The parameters p, q and s are dependent on material elastic constants and the relations can be found in Sih and Liebowitz [22]. The details of obtaining the stiffness matrix has also been given in Appendix A. Using the expressions for u and v in the above equations, rotations about the z-axis can be calculated as

$$\omega_{xy} = \frac{1}{2}\left[\frac{\partial v}{\partial x} - \frac{\partial u}{\partial y}\right] \tag{4}$$

The expressions for obtaining the deformation gradients $\left(\frac{\partial v}{\partial x}, \frac{\partial u}{\partial y}\right)$ are given in Appendix B.

After we find the maximum tensile stress in the struts near the crack tip, we can use Eq. (1) to obtain the Mode-I fracture toughness of the foam. For Mode-II fracture toughness, we use K_{II} and K_{IIc} in Eq. (1) instead of K_I and K_{Ic}.

3. FEM model of the unit cell

The tetrakaidecahedral unit cell that we propose to study is a 14-sided polyhedron with six square and eight hexagonal faces. It is more precisely called truncated octahedron, since it is created by truncating the corners of an octahedron [23]. From a different viewpoint, it can be generated by truncating the corners of a cube [7]. All the edges of the cell are of equal length L and cross sectional area A as shown in Fig. 4. The tetrakaidecahedral foam has a BCC lattice structure. The axes of the BCC lattice are parallel to the axes of the cube. Due to the symmetry of the structure, the Young's moduli of the foam in the lattice vector directions are equal:

$$E^*_{001} = E^*_{010} = E^*_{100} \tag{5}$$

Each strut of the cell is treated as a beam element. In our study, the cross section of the struts is assumed to be an equilateral triangle with side length D (Fig. 4). Similar foam with triangular cross section was studied by Zhu et al. [7]. The triangular cross section is considered closer to the three-cusp hypocycloid cross section of polyurethane foams as was shown by Sullivan et al. from their microstructure studies [24]. In the finite element analysis we need to input numerical values for the solid material properties. The properties used in this study are given in Table 1.

We use the finite element based micromechanical analysis described by Thiyagasundaram et al. [25] to calculate the homogeneous elastic constants of the foam. One can also use the analytical expressions derived by Zhu et al. [7]. The calculated properties are given in Table 2. These properties were used to calculate the compliance coefficients in Eq. (A1) in Appendix A. We have used the two-node Euler–Bernoulli (B33) beam elements in ABAQUS 6.9–2 to model the struts.

4. Results and discussion

The procedures described in Section 2 were used to predict the Mode I, Mode II and mixed mode fracture toughness of the foam. Since we are interested in plane strain fracture toughness only one unit cell was used in the thickness direction (z-direction). Periodic boundary conditions were imposed on the two surfaces normal to the z-axis.

4.1. Mode-I and Mode-II fracture toughness

A convergence study was performed by calculating the fracture toughness choosing micromechanical models of different sizes. The size of the model is varied by increasing the number of unit cells chosen along the x and the y directions.

Table 3
Mode-I fracture toughness results with Input $K_I = 100$.

Case	Model width (cells)	Model height (cells)	Crack length (cells)	Total number of nodes	Strut tip stress (MPa)		Fracture toughness ($Pa\sqrt{m}$)		Difference between values with and without rotation (%)
					W/O rotation	With rotation	W/O rotation	With rotation	
1	10	11	5	1844	112	111.5	615.4	618.2	0.45
2	12	13	6	2596	111.6	111.3	617.6	619.8	0.35
3	14	15	7	3476	111.5	111.2	618.7	620.1	0.22
4	16	17	8	4484	111.3	111.2	619.4	620.2	0.12
5	18	19	9	5620	111.2	110.9	620.2	621.5	0.21
6	20	21	10	6884	111.1	110.9	620.7	621.7	0.17
7	22	23	11	8276	111	110.8	621.2	622.1	0.14
8	24	25	12	9796	110.9	110.8	621.6	622.5	0.14
9	26	27	13	11,444	110.8	110.7	622.1	623	0.14
10	28	29	14	13,220	110.8	110.7	622.1	622.9	0.13
11	30	31	15	15,124	110.8	110.7	622.1	622.8	0.11
12	32	33	16	17,156	110.8	110.7	622.2	622.7	0.09
13	34	35	17	19,316	110.8	110.7	622.1	622.7	0.10

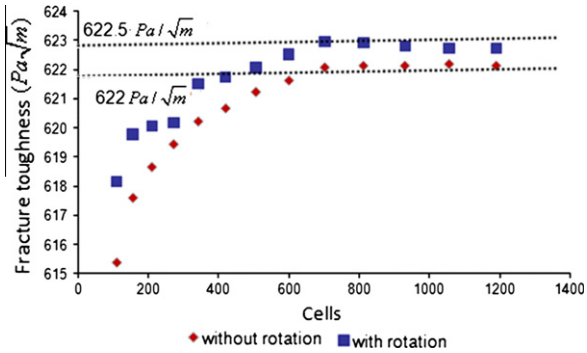

Fig. 6. Mode-I fracture toughness convergence.

In the current study, two sets of boundary conditions have been considered, one which does not include rotations ω_{xy} as boundary condition and the other which includes rotations. The question of including rotation arises because of the fact that beam elements are used to model the foam in the vicinity of the crack tip and the beam element nodes have rotation as a degree of freedom. In the previous work Choi and Sankar [17] ignored the rotations basically setting the corresponding couple to be equal to zero. On the other hand Schmidt and Fleck [20] included the rotation as a boundary condition. In the present study we considered both cases – with and without rotation boundary condition.

Thirteen different models were considered to check convergence for Mode I. Four models out of the 13 models are shown in Fig. 5. The crack size is 50% of the width in all the cases chosen. The results obtained have been shown in Table 3. The total number of nodes in the models varies from 1800 to almost 20,000 nodes respectively as shown in the Table 3. It is seen that as the size of the model is increased, there is convergence (Fig. 6).

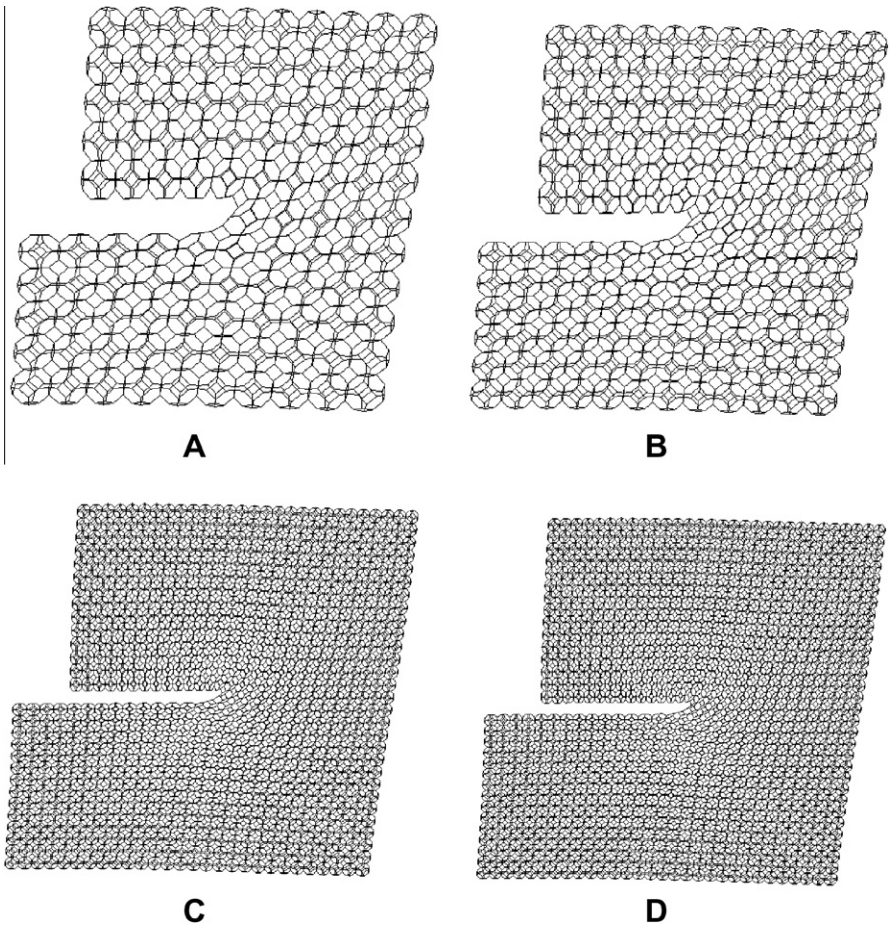

Fig. 7. Mode-II fracture – deformed configurations. (A) 10(w) × 11(h), (B) 12(w) × 13(h), (C) 28(w) × 29(h), and (D) 30(w) × 31(h).

Table 4
Mode-II fracture toughness results with Input K_{II} = 100.

Case no.	Model width (cells)	Model height (cells)	Crack length (cells)	Total number of nodes	Strut tip stress (MPa)		Fracture toughness ($Pa\sqrt{m}$)		Difference between values with and without rotation (%)
					W/O rotation	With rotation	W/O rotation	With rotation	
1	10	11	5	1844	125.1	125	551	551.6	0.112
2	12	13	6	2596	126.4	126.3	545.3	546.1	0.135
3	14	15	7	3476	127.4	127.2	541.4	542	0.118
4	16	17	8	4484	127.8	127.6	539.6	540.2	0.11
5	18	19	9	5620	128.1	128	538.2	538.8	0.109
6	20	21	10	6884	128.8	128.6	535.4	536.1	0.124
7	22	23	11	8276	129.4	129.3	532.8	533.4	0.116
8	24	25	12	9796	130.8	130.6	527.2	527.8	0.115
9	26	27	13	11,444	131.4	131.2	524.9	525.6	0.13
10	28	29	14	13,220	131.6	131.5	523.9	524.3	0.076
11	30	31	15	15,124	131.8	131.8	523	523.3	0.068
12	32	33	16	17,156	131.9	131.9	522.7	522.9	0.046
13	34	35	17	19,316	132	131.9	522.5	522.7	0.045

The results show that for foam with relative density 0.16% (Table 3, Fig. 6) the Mode-I fracture toughness converges to 622 $Pa\sqrt{m}$ when rotational boundary conditions are not applied and to 622.5 $Pa\sqrt{m}$ when the rotations are applied. The highest and the lowest fracture toughness values are 622.2 $Pa\sqrt{m}$ and 615.4 $Pa\sqrt{m}$, respectively which makes the maximum variation to be only about 1.1%. This would mean that calculated value can be used as a material property. Also since the variation in the converged fracture toughness values between fracture toughness with and without rotational BC is only 0.1%, it can be concluded that there is no significant change in fracture toughness values when rotations are applied.

Similar to the procedure for Mode I, by imposing the displacements of K_{II} field on the boundary to micromechanical model (Eqs. (2) and (3)) we can obtain the maximum tensile stress near the crack tip from the FE results and hence calculate the Mode-II fracture toughness value using Eq. (4). Again a convergence study is conducted by calculating the fracture toughness

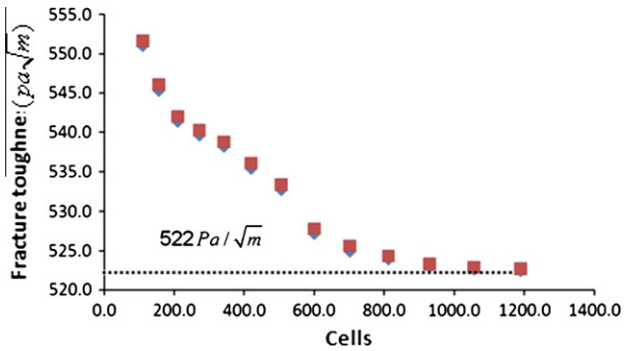

Fig. 8. Mode-II fracture toughness convergence.

Table 5
Results obtained for mixed mode fracture toughness (30 × 31 configuration).

ψ (deg)	K_I ($Pa\sqrt{m}$)	K_{II} ($Pa\sqrt{m}$)	Critical strain energy release rate G_c (N/m)
0	622.8	0.0	8.31
5	641.8	56.2	8.89
10	656.2	115.7	9.51
15	658.9	176.5	9.96
20	660.8	240.5	10.59
30	639.6	369.3	11.68
40	591.6	496.4	12.77
45	559.3	559.3	13.40
50	522.5	622.6	14.15
60	390.3	676.0	13.05
70	234.4	644.1	10.06
80	105.0	595.4	7.83
85	49.1	561.5	6.80
90	0.0	523.0	5.86

choosing different micromechanical model sizes. As for the case of Mode I, the size of the model is varied by increasing the number of unit cells chosen along the x and the y directions. Similar to Mode I, two sets of cases have been considered – one which does not include rotations as boundary conditions and the other which includes rotations. Deformed configurations of

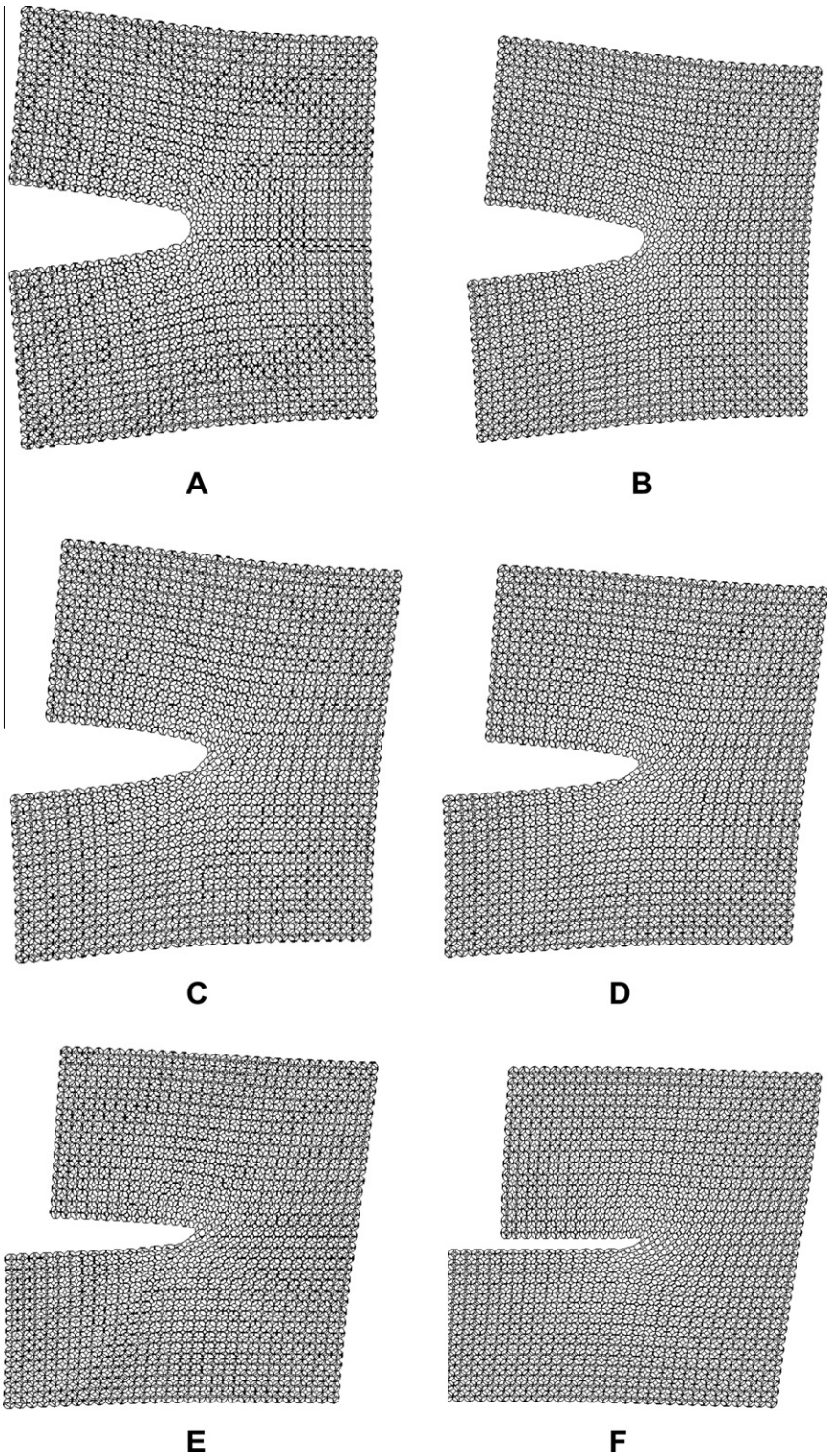

Fig. 9. Mixed mode fracture toughness – deformed configurations (30×31). (A) $\psi = 0$, (B) $\psi = 15$, (C) $\psi = 30$, (D) $\psi = 45$, (E) $\psi = 60$, and (F) $\psi = 90$.

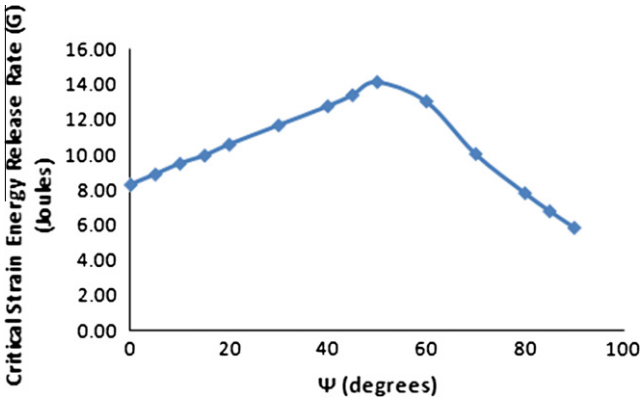

Fig. 10. Mixed mode fracture toughness results (30×31 configuration).

a few models chosen for this study are shown in Fig. 7. The results obtained are presented in Table 4 and convergence has been shown in Fig. 8.

The results show that the Mode-II fracture toughness converges to about 522 $\mathrm{Pa}\sqrt{\mathrm{m}}$ when rotational displacements are not applied and to 521.5 $\mathrm{Pa}\sqrt{\mathrm{m}}$ when the rotations are applied. The highest and the lowest fracture toughness values are 551.6 $\mathrm{Pa}\sqrt{\mathrm{m}}$ and 521.7 $\mathrm{Pa}\sqrt{\mathrm{m}}$ respectively which makes the maximum variation about 5.3%. Also since the variation in the converged fracture toughness values between fracture toughness with and without rotational BCs is only 0.1%, there seems to be no significant change in fracture toughness values when rotations are applied.

4.2. Mixed mode fracture toughness

In calculating mixed mode fracture toughness, two stress intensity factors are required as input for calculation of boundary displacements. The Mode I and Mode II to stress intensity factors were varied as

$$K_{\mathrm{II}} = K_{\mathrm{I}} \tan\psi, \quad (0 \leqslant \psi \leqslant \frac{\pi}{2}) \tag{6}$$

where ψ is the phase angle, a measure of mode mixity. One can note that $\psi = 0$ corresponds to pure Mode I and $\psi = \frac{\pi}{2}$ to Mode II. Intermediate values of ψ indicate mixed mode fracture. All the other equations for calculating displacements and rotations remain the same as given in the appendices.

Results obtained from simulations for predicting mixed mode fracture toughness are shown in Table 5. Some deformed configurations for different combinations of K_{I} and K_{II} are shown in Fig. 9. The size of the local region is assumed to be 30×31 cells. In order to present the mixed mode fracture toughness results we use the total critical energy release rate G_c as a measure of effective fracture toughness and plot is as a function of the phase angle ψ in Fig. 10. We use the isotropic material formula for G_c given by

$$G_c = \frac{K_{\mathrm{I}}^2 + K_{\mathrm{II}}^2}{E} \tag{7}$$

where E is the Young's modulus of the foam, say E_x. It should be noted from the results in Table 2 that the foam is nearly isotropic, and the use of the above formula in Eq. (7) is justified at least for qualitative understanding of the effect of mode mixity on the fracture toughness. From Fig. 10 one can note that the fracture toughness increases as the phase angle increases from 0-degree and reaches a maximum value at about $\psi = 50^{\circ}$.

5. Summary and conclusion

A finite element based method has been used to calculate the fracture toughness of foams. The inputs to the model are the geometric parameters required to model the repeating unit cell and tensile strength of the foam ligament or strut. A micromechanics based method has been used to calculate the Mode I, Mode II and Mixed mode fracture toughness of foams with tetrakaidecahedral unit cells. Fracture toughness has been shown to converge as the size of micromechanical model is increased. Hence, the calculated fracture toughness can be used as a material property. It has also been shown that applying rotation boundary conditions does not influence the calculated fracture toughness significantly, at least for the cases considered here.

Acknowledgements

The Florida Space Grants Consortium's FSREGP Program supported this research. The authors gratefully acknowledge the interest and encouragement of Dr. Jaydeep Mukherjee, Director of NASA Florida Space Grants Consortium and Interim Director of Florida Space Institute.

Appendix A

The compliance matrix [S] of a plane orthotropic medium is given by

$$[S]=\begin{bmatrix} S_{11} & S_{12} & S_{16} \\ S_{21} & S_{22} & S_{26} \\ S_{16} & S_{26} & S_{66} \end{bmatrix}=\begin{bmatrix} 1/E_x & -v_{xy}/E_y & 0 \\ -v_{xy}/E_x & 1/E_y & 0 \\ 0 & 0 & 1/G_{xy} \end{bmatrix} \tag{A1}$$

where the elastic constants in the above equation can be obtained from Table 2.

The characteristic equation of the orthotropic material as given by Sih and Liebowitz [22]

$$S_{11}\mu^4-2S_{16}\mu^3+(2S_{12}+S_{66})\mu^2-2S_{26}\mu+S_{22}=0 \tag{A2}$$

There are four roots of the above characteristic equation. We denote s_1 and s_2 as the two unequal roots with positive conjugate values:

$$s_1=\mu_1=\alpha_1+\mathbf{i}\beta_1,\quad s_2=\mu_2=\alpha_2+\mathbf{i}\beta_2 \tag{A3}$$

The constants p_j and q_j (j = 1, 2) are related s_1 and s_2 as below

$$p_1=S_{11}s_1^2+S_{12}-S_{16}s_1,\quad p_2=S_{11}s_{21}^2+S_{12}-S_{16}s_2 \tag{A4}$$
$$q_1=\frac{S_{12}s_1^2+S_{22}-S_{26}s_1}{s_1},\ q_2=\frac{S_{12}s_2^2+S_{22}-S_{26}s_2}{s_2}$$

The displacement field in the vicinity of crack tip is a function of the orthotropic material parameters p_1, p_2, q_1, q_2, s_1 and s_2 as given in Eqs. (2) and (3).

Appendix B

The procedures for calculating rotation boundary conditions (ω_{xy}) are as follows. From the displacement field given in Eq (2) we can calculate displacement gradients for Mode I as:

$$\begin{aligned}
\frac{\partial u}{\partial r}&=K_{\mathrm{I}}\left(\frac{1}{\sqrt{2\pi r}}\right)\mathrm{Re}\left\{\frac{1}{s_1-s_2}\left[s_1p_2(\cos\theta+s_2\sin\theta)^{1/2}-s_2p_1(\cos\theta+s_1\sin\theta)^{1/2}\right]\right\}\frac{\partial u}{\partial\theta}\\
&=K_{\mathrm{I}}\sqrt{\frac{2r}{\pi}}\mathrm{Re}\left\{\frac{1}{s_1-s_2}\left[\tfrac{s_1p_2}{2}(\cos\theta+s_2\sin\theta)^{-1/2}(-\sin\theta+s_2\cos\theta)-\tfrac{s_2p_1}{2}(\cos\theta+s_1\sin\theta)^{-1/2}(-\sin\theta+s_1\cos\theta)\right]\right\}\frac{\partial v}{\partial r}\\
&=K_{\mathrm{I}}\left(\frac{1}{\sqrt{2\pi r}}\right)\mathrm{Re}\left\{\frac{1}{s_1-s_2}\left[s_1q_2(\cos\theta+s_2\sin\theta)^{1/2}-s_2q_1(\cos\theta+s_1\sin\theta)^{1/2}\right]\right\}\frac{\partial v}{\partial\theta}\\
&=K_{\mathrm{I}}\sqrt{\frac{2r}{\pi}}\mathrm{Re}\left\{\frac{1}{s_1-s_2}\left[\tfrac{s_1q_2}{2}(\cos\theta+s_2\sin\theta)^{-1/2}(-\sin\theta+s_2\cos\theta)-\tfrac{s_2q_1}{2}(\cos\theta+s_1\sin\theta)^{-1/2}(-\sin\theta+s_1\cos\theta)\right]\right\}
\end{aligned} \tag{A5}$$

The displacement gradients for Mode II can be derived in a similar fashion:

$$\begin{aligned}
\frac{\partial u}{\partial r}&=K_{\mathrm{II}}\left(\frac{1}{\sqrt{2\pi r}}\right)\mathrm{Re}\left\{\frac{1}{s_1-s_2}\left[p_2(\cos\theta+s_2\sin\theta)^{1/2}-p_1(\cos\theta+s_1\sin\theta)^{1/2}\right]\right\}\frac{\partial u}{\partial\theta}\\
&=K_{\mathrm{II}}\\
&\quad\times\sqrt{\frac{2r}{\pi}}\mathrm{Re}\left\{\frac{1}{s_1-s_2}\left[\tfrac{p_2}{2}(\cos\theta+s_2\sin\theta)^{-1/2}(-\sin\theta+s_2\cos\theta)-\tfrac{p_1}{2}(\cos\theta+s_1\sin\theta)^{-1/2}(-\sin\theta+s_1\cos\theta)\right]\right\}\frac{\partial v}{\partial r}\\
&=K_{\mathrm{II}}\left(\frac{1}{\sqrt{2\pi r}}\right)\mathrm{Re}\left\{\frac{1}{s_1-s_2}\left[q_2(\cos\theta+s_2\sin\theta)^{1/2}-q_1(\cos\theta+s_1\sin\theta)^{1/2}\right]\right\}\frac{\partial v}{\partial\theta}\\
&=K_{\mathrm{II}}\sqrt{\frac{2r}{\pi}}\mathrm{Re}\left\{\frac{1}{s_1-s_2}\left[\tfrac{q_2}{2}(\cos\theta+s_2\sin\theta)^{-1/2}(-\sin\theta+s_2\cos\theta)-\tfrac{q_1}{2}(\cos\theta+s_1\sin\theta)^{-1/2}(-\sin\theta+s_1\cos\theta)\right]\right\}
\end{aligned} \tag{A6}$$

The rotational boundary condition can be calculated as:

$$\frac{\partial v}{\partial x} = \cos\theta\left(\frac{\partial v}{\partial r}\right) - \frac{\sin\theta}{r}\left(\frac{\partial v}{\partial \theta}\right)\frac{\partial u}{\partial y} = \sin\theta\left(\frac{\partial u}{\partial r}\right) + \frac{\cos\theta}{r}\left(\frac{\partial u}{\partial \theta}\right)\omega_{xy} = \frac{1}{2}\left[\frac{\partial v}{\partial x} - \frac{\partial u}{\partial y}\right] \tag{A7}$$

References

[1] Thompson W. On the division of space with minimum partitional area. Philos Mag 1887;24:503–900.
[2] Weaire D, Phelan R. A counterexample to Kelvin conjecture on minimal-surfaces. Philos Mag Lett 1994;69:107–10.
[3] Hall RB, Hager JW. Performance limits for stiffness-critical graphitic foam structures. 1. Comparisons with high-modulus foams, refractory alloys and graphite–epoxy composites. J Compos Mater 1996;30:1922–37.
[4] Lee S, Wang J, Sankar BV. A micromechanical model for predicting the fracture toughness of functionally graded foams. Int J Solids Struct 2007;44:4053–67.
[5] Li K, Gao XL, Roy AK. Micromechanics model for three-dimensional open-cell foams using a tetrakaidecahedral unit cell and Castigliano's second theorem. Compos Sci Technol 2003;63:1769–81.
[6] Li K, Gao XL, Roy AK. Micromechanical modeling of three-dimensional open-cell foams using the matrix method for spatial frames. Compos Part B – Engng 2005;36:249–62.
[7] Zhu HX, Knott JF, Mills NJ. Analysis of the elastic properties of open-cell foams with tetrakaidecahedral cells. J Mech Phys Solids 1997;45:319.
[8] Ridha M, Shim VPW, Yang LM. An elongated tetrakaidecahedral cell model for fracture in rigid polyurethane foam. Fract Strength Solids VI 2006;306–308(Pts. 1 and 2):43–8.
[9] Laroussi M, Sab K, Alaoui A. Foam mechanics: nonlinear response of an elastic 3D-periodic microstructure. Int J Solids Struct 2002;39:3599–623.
[10] Maiti SK, Ashby MF, Gibson LJ. Fracture-toughness of brittle cellular solids. Scr Metall 1984;18:213–7.
[11] Huang JS, Gibson LJ. Fracture-toughness of brittle foams. Acta Metall Mater 1991;39:1627–36.
[12] Huang JS, Gibson LJ. Fracture-toughness of brittle honeycombs. Acta Metall Mater 1991;39:1617–26.
[13] Brezny R, Green DJ. The effect of cell-size on the mechanical-behavior of cellular materials. Acta Metall Mater 1990;38:2517–26.
[14] Brezny R, Green DJ. Factors controlling the fracture-resistance of brittle cellular materials. J Am Ceram Soc 1991;74:1061–5.
[15] Brezny R, Green DJ, Dam CQ. Evaluation of strut strength in open-cell ceramics. J Am Ceram Soc 1989;72:885–9.
[16] Gibson LJ, Ashby MF. Cellular solids: structure and properties. UK: Cambridge University Press; 1997.
[17] Choi S, Sankar BV. Fracture toughness of carbon foam. J Compos Mater 2003;37:2101–16.
[18] Choi S, Sankar BV. A micromechanical method to predict the fracture toughness of cellular materials. Int J Solids Struct 2005;42:1797–817.
[19] Wang J. Fracture toughness of cellular materials using finite element based micromechanics. Doctoral Dissertation. University of Florida, Gainesville, Florida; 2007.
[20] Schmidt I, Fleck NA. Ductile fracture of two dimensional cellular structures. Int J Fract 2001;111:327–42.
[21] Fleck NA, Qiu X. The damage tolerance of elastic–brittle, two dimensional isotropic lattices. J Mech Phys Solids 2007;55:562–88.
[22] Sih GC, Liebowitz H. Mathematical theories of brittle fracture. New York and London: Academic Press; 1968.
[23] Weisstein EW. Truncated octahedron. MathWorld – A Wolfram web resource. <http://mathworld.wolfram.com/TruncatedOctahedron.html>.
[24] Sullivan RM, Ghosm LJ, Lerch BA, 2008. Application of an elongated Kelvin model to space shuttle foams. AIAA Paper 2008-1786. In: The proceedings of the 49th AIAA/ASME/ASCE/AHS/ASC structures, structural dynamics, and materials. Reston (VA): AIAA.
[25] Thiyagasundaram P, Sankar BV, Arakere NK. Elastic properties of open-cell foams with tetrakaidecahedral cells using finite element analysis. AIAA J 2010;48(4):818–28.